Inorganic Chemistry

Article

pubs.acs.org/IC

Atomistic Modeling of the Low-Temperature Atom-Beam Deposition of Magnesium Fluoride

Sridhar Neelamraju,*[,†,‡] Johann Christian Schön,[†] and Martin Jansen[†]

[†]Max Planck Institute for Solid State Research, Heisenbergstrasse 1, D-70569 Stuttgart, Germany

ABSTRACT: We model the deposition and growth of MgF_2 on a sapphire substrate as it occurs in a low-temperature atom-beam-deposition experiment. In the experiment, an (X-ray) amorphous film of MgF_2 is obtained at low temperatures of 170−180 K, and upon heating, this transforms to the expected rutile phase via the $CaCl_2$-type structure. We confirm this from our simulations and propose a mechanism for this transformation. The growth process is analyzed as a function of the synthesis parameters, which include the substrate temperature, deposition rate of clusters, and types of clusters deposited. Upon annealing an initially amorphous deposit, we observe the formation of two competing nanocrystalline modifications during this process, which exhibit the $CaCl_2$ and CdI_2 structure types, respectively. We argue that this joint growth of the two nanocrystalline polymorphs stabilizes the kinetically unstable $CaCl_2$-type structure on the macroscopic level long enough to be observed in the experiment.

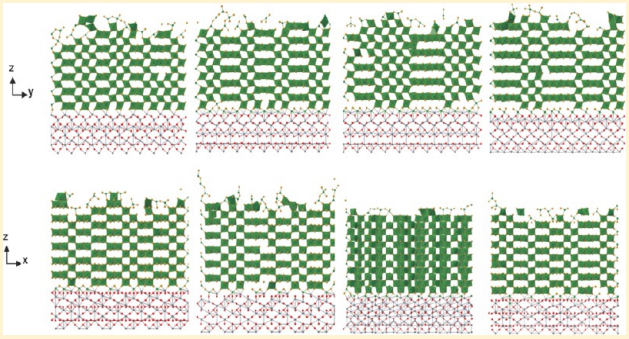

INTRODUCTION

The thermodynamically stable and metastable modifications of bulk solids can readily be predicted by analyzing their energy landscape,[1−9] yet frequently their synthesis results in a metastable polymorph instead,[10−15] or, conversely, one only succeeds in generating the thermodynamically stable state but none of the metastable modifications. The reason is that most crystallization mechanisms are actually controlled by the kinetics of the atomic processes through which nucleation, crystal growth, and phase transformations occur. Closely related is the observation that different experimental techniques for the synthesis of a chemical compound take different paths to the global minimum structure, along which various metastable intermediates may appear. Conversely, one can reach such modifications by purposefully selecting special synthesis methods.

For example, the low-temperature atom-beam-deposition (LT-ABD) method[16] has been employed in order to produce novel stable and metastable phases of alloys,[17] nitrides,[11] and halides[18,19] that had not been accessible using any alternative synthesis routes. This method proceeds by deposition of an amorphous film of the reactants from the gas phase at low temperatures, followed by slow heating and tempering of the deposit until one or more (meta)stable modifications crystallize. A plausible reason for the success of this technique might be the existence of an atomically disperse deposit generated during the deposition stage and thus the short diffusion times needed before the different atoms can react. Because of the rather low thermal activation barrier associated with this reaction step, the synthesis can take place at low temperatures (thus preserving possible metastable products), and development of the product takes place on experimentally observable time scales. However, many aspects of this synthesis are still unresolved, especially the genesis and structure of the amorphous deposit and the nucleation and growth processes involved in the formation of crystalline phase(s). In earlier work,[20] we analyzed the deposition and growth of xenon films via the LT-ABD method. However, the processes involved in the synthesis of ionic compounds are expected to be considerably more complex, requiring further study.

EXPERIMENTAL SECTION

Recently, a new $CaCl_2$-type polymorph of MgF_2 has been synthesized using the LT-ABD technique.[21] In this experiment, a MgF_2 bulk crystal (in the rutile modification) was evaporated to form a gaseous phase, using thermal effusion cells at constant temperatures ranging from 1300 to 1500 K and at very low partial pressures of 10^{-6} mbar. The gas produced was then deposited on a cold substrate, which was maintained at low temperatures (170−180 K), resulting in an X-ray amorphous deposit on the substrate. After slow heating of the substrate from the bottom, the new (meta)stable $CaCl_2$-type modification was obtained, which upon subsequent tempering at high temperatures converted into the known rutile modification of MgF_2. While the existence of new metastable modifications of MgF_2 in general had already been predicted 15 years ago,[22−24] it is rather surprising that this particular polymorph of MgF_2 appears to be stable at standard pressure and low temperatures because careful local optimization on the ab initio level show that a bulk periodic $CaCl_2$-type polymorph of MgF_2 is not kinetically stable and directly relaxes to the well-known thermodynamically stable rutile-type arrangement (via a shear movement corresponding to a C_2-axis rotation).[25,26] Employ-

Special Issue: To Honor the Memory of Prof. John D. Corbett

Received: July 7, 2014
Published: September 23, 2014

   dx.doi.org/10.1021/ic501499k | Inorg. Chem. 2015, 54, 782−791

ing only experimental measurement tools cannot resolve this contradiction, and thus it is necessary to theoretically study the mechanism that stabilizes this arrangement in MgF_2 during the LT-ABD synthesis, by performing simulations that mimic the experiment as closely as possible.

Thus, in this molecular dynamics (MD) study, we strive to model the LT-ABD synthesis of MgF_2 in detail. Besides trying to clarify the reason for the stability of the $CaCl_2$ structure type in the LT-ABD experiment described above, our main goal is to further our understanding of this synthesis procedure in atomistic detail because of the unusually high degree of control over the synthesis parameters available with this technique. Because the composition of the gas phase is expected to play an important role in the case of ionic systems, the current study was preceded by a detailed theoretical investigation of the MgF_2 gas phase using energy-landscape explorations to identify possible molecules in the gas phase[27] and ab initio methods to compute their Raman spectra for comparison with the experiment. This was complemented by the experimental determination of the Raman spectra of the existing $(MgF_2)_n$ clusters by freezing-out the gas phase present during the LT-ABD experiment.[25]

METHOD

The model system we employ for the description of LT-ABD consists of a substrate, which is modeled as several layers of substrate atoms, and a gas phase that slowly rains down upon the substrate. During the deposition process, the bottom layers of the substrate are kept at a fixed temperature while the temperature of the upper substrate layers and of the deposited atoms are free to adjust. In particular, cooling and heating only takes place via the bottom of the substrate. Several substrates and different gas-phase compositions are used during the simulations, and furthermore the temperature of the substrate and the deposition rate are varied between runs. After the deposition phase has ended, tempering simulations at various temperatures are performed. Both during the deposition and during the annealing, several quantities, such as the temperature as a function of the location in the deposit and long-range and local order in the deposited film, were kept track of and analyzed.

Model Potential. The potential chosen to describe the Al_2O_3 and MgF_2 systems was a Coulomb-plus-Buckingham-type potential derived by Bacorisen et al.[28] for Al_2O_3 and by Catti et al.[29] for MgF_2, respectively. The interactions between the substrate (Al_2O_3) and the vapor phase (clusters of MgF_2) were described by a Coulomb-plus-Lennard-Jones-type potential. The potential for MgF_2 had originally been derived to reproduce the lattice constants and elastic constants of the bulk MgF_2 rutile structure. However, we have previously shown that even for clusters the potential qualitatively and partly quantitatively reproduces the ab initio energy landscape of the $(MgF_2)_3$ trimer including the sub-basins,[27] and thus the potential should be of sufficient quality to describe the deposition and annealing processes that are to be modeled. Given that our system is periodic in two dimensions, treatment of the Coulomb term in the Coulomb-plus-Buckingham-type potential within the Ewald scheme was computationally too expensive. Therefore, we opted for the damping procedure proposed by Wolf et al.,[30] which has the advantage of being applicable to systems with arbitrary geometry, without introducing a significant error in the potential calculation. Also, given the scale of this simulation, we implemented the fast pair-list construction algorithm, as described by Heinz and Hünenberger.[31] Finally, in the Coulomb-plus-Lennard-Jones interaction between the Mg and F atoms, on the one hand, and the Al and O atoms in the substrate, on the other hand, the ϵ term was fixed at 0.01 eV and the σ terms were derived from the sum of the ionic distances[32] (σ_{Mg} = 0.78 Å, σ_F = 1.33 Å, σ_{Al} = 0.57 Å, and σ_O = 1.2 Å). The precise value of the strength of the Lennard-Jones-type potential is not expected to play a significant role because the Coulomb term typically dominates the Lennard-Jones term in ionic compounds.[33] The parameters of the potentials are given in Table 1.

Table 1. Potential Parameters for the Coulomb-plus-Buckingham-Type Potential Used for MD Simulations

i, j	A (eV)	ρ (Å)	C (Å eV)
Mg−F	905.517	0.215	0.5557
F−F	17039.097	0.215	15.168
Mg−Mg	4166.274	0.215	0.5557
Al−O	1374.79	0.301	0.0
O−O	9547.96	0.219	32.0

Substrates. Depositions were carried out on three different slabs: α-Al_2O_3 (0001), MgF_2-rutile (100 and 110 surfaces), and MgF_2 anatase (011 and 100 surfaces); cf. Figure 1. In each case, the slab was oriented such that the topmost layer of the slab had a z-coordinate of zero, and the slab was periodically repeated in the xy direction.

The α-Al_2O_3 slab comprised 3600 atoms and was obtained by constructing a hexagonal close packed (hcp) type stacking of planes of O atoms, where the Al atoms were inserted at the appropriate octahedral holes. Six close-packed planes consisting of 360 O atoms each and with lateral dimensions of 48.5 Å × 50.40 Å were used. The nearest-neighbor Al−O distance was 2.8 Å. It has been shown in ultrahigh-vacuum experiments that this substrate is O-terminated in the presence of major impurities such as argon, nitrogen, and water.[34,35] Because the pressure in the experimental chamber before starting deposition was around 10^{-8} mbar and the substrate had not been specially treated with any cleaning process, we expected the exposed Al layer to be passivated with O and other species present in the chamber. Therefore, it is reasonable to assume an O-terminated surface as a starting configuration before deposition.

The MgF_2 rutile slab was stabilized with the (100) and (110) surfaces exposed. The (100) slab comprised 3168 atoms, and the dimensions were 48.84 Å × 50.87 Å. For the (110) slab, 3624 atoms were used, and the slab's dimensions were 51.88 Å × 52.32 Å in the x and y directions, respectively. Both surfaces were F-terminated. The two MgF_2-anatase slabs consisted of 3360 [(011) surface exposed] and 3120 [(100) surface exposed] atoms with dimensions of 53.50 Å × 52.21 and 48.59 Å × 49.69 Å, respectively. These surfaces were chosen on the basis of previous studies on the analogous TiO_2 rutile and anatase surfaces.[36]

In all cases, the initial slab was locally minimized by using a MD-assisted quenching procedure. At each MD iteration, after the classical equations of motion was solved via the velocity−Verlet algorithm, a quench was performed by canceling all of the components of an atom's velocity whose scalar product with the force acting on the atom were negative. Periodic boundary conditions across the xy plane were applied. Typically, we observe an inward relaxation of the topmost layer of O atoms in Al_2O_3 and, to a lesser extent, of the F atoms on MgF_2 such that the surface dipole moment is reduced.

Next, the first six atom layers of the slab from the bottom were fixed in order to reproduce the effect of the infinite

dx.doi.org/10.1021/ic501499k | Inorg. Chem. 2015, 54, 782−791

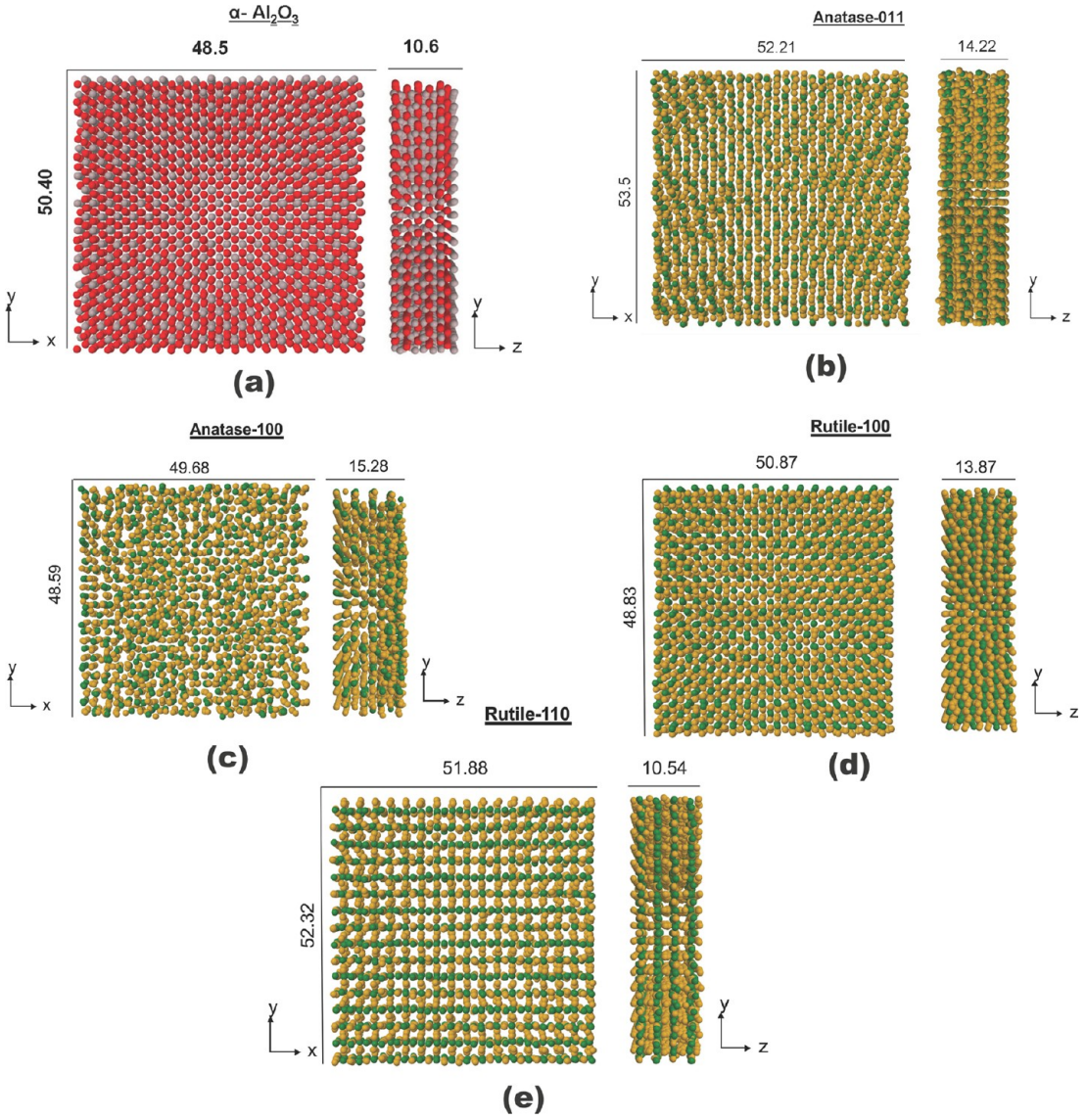

Figure 1. Five substrates on which depositions were carried out (dimensions are in Å): (a) α-Al_2O_3; (b) MgF_2-anatase (011); (c) MgF_2-anatase (001); (d) MgF_2-rutile (100); (e) MgF_2-rutile (110). Color scheme: Mg, green; F, yellow; Al, gray; O, red.

extension of the substrate in the positive z direction. A velocity rescaling thermostat was applied to the remaining atoms of the slab, and the slabs were equilibrated at temperatures ranging from 10 to 1000 K. During computation of the average temperature within a layer, bins along the z direction of a thickness of 4 Å were chosen, in order to make sure that at least 100 atoms were involved in the computation of the average kinetic energy per layer. The temperature of the layer is then calculated from the kinetic energy via the law of equipartition of energy.

The initial distance of the to-be-deposited particles from the growing surface was fixed and typically set to a value of about 10 Å. The lateral position of the center of mass of the impinging cluster was randomly chosen, and the clusters were provided with an initial kinetic energy of 2 meV. Analogous to the experiment, depositions were carried out at temperatures ranging from 50 to 1000 K. Several sizes of clusters were used for the deposition, with most of the work done using a combination of monomers and dimers (ratio 1:1). Other compositions that were deposited were a mixture of $(MgF_2)_{15}$ and $(MgF_2)_{10}$ clusters (in a 4:1 ratio) and one with only the MgF_2 linear monomer. The sequence of monomers and D_{2h} dimers to be deposited was randomly generated with a probability of $^1/_2$ for each cluster type, at two different deposition rates of 10^{12} and 10^{10} atoms/s. Of course, these deposition rates are much faster than the rate used in the experiment. In order to check the variability of the outcome of the simulations, the depositions using the monomer−dimer mixture were repeated for three different random seeds used for generating the sequence of clusters during the deposition.

RESULTS AND DISCUSSION

Preliminary Work. *Results of Earlier Cluster and Gas-Phase Analysis.*[25,27] The gas phase present in the deposition experiment was explored in detail in two previous investigations.[25,27] In the first study,[27] we generated many low-energy neutral isomers of $(MgF_2)_n$ clusters of sizes of up to $(MgF_2)_{10}$ using a combination of simulated annealing[37] and the threshold algorithm.[38] On the basis of analysis of the energetic barriers between the various isomers on the landscape of small

dx.doi.org/10.1021/ic501499k | Inorg. Chem. 2015, 54, 782−791

MgF_2 clusters and the mean free path inside the apparatus, we surmised that it is unlikely that isomerization would occur once the cluster has been formed in the gas phase. Next, on the basis of Raman and IR spectra computed using ab initio methods, we investigated the gas phase present in the actual experiment. By comparing experimental Raman measurements with our calculations, we were able to confirm the existence of the MgF_2 monomer and the D_{2h} dimer[25] in the experimental apparatus, together with the possible existence of ionic clusters. On the basis of these results, we modeled the gas phase for most of the deposition simulations as consisting of a mixture of the linear monomer and the D_{2h} dimer.

Effects of Impurity Layers on the Substrate on the Synthesis Processes. A major concern during the LT-ABD experiment is the presence of impurities in the chamber and their effect on the deposition process and the subsequent amorphous-to-crystalline transition. Even at the low pressures achieved in the deposition chamber, one expects a covering of the substrate surface with various gas molecules. In order to analyze the effects of such a layer of neutral gas atoms and molecules on the synthesis process, we have modeled this impurity layer as a monolayer of Xe atoms, for simplicity, because we do not expect significant chemical reactions between the gas molecules and the substrate to occur.[39]

In practice, we deposited 119 Xe atoms onto the MgF_2-rutile substrate of 3600 atoms at 50 K and at a rate of 10^{10} atoms/s. After deposition, the Xe atoms were allowed to equilibrate on the MgF_2 surface at 50 K for 15 ns. Finally, the substrate was annealed at 1000 K for 30 ns, whereupon most of the Xe atoms evaporated into the gas phase (see Figure 2). Next, we deposited a mixture of the monomer and the dimer of MgF_2 (6648 atoms, at a rate of 10^{11} atoms/s, at a temperature of 50 K) onto this layer of Xe. We observed that some of the Xe atoms evaporated during this deposition process, while the rest were incorporated into the growing amorphous MgF_2 deposit. Upon annealing this deposit at 1500 K, we found that most of the remaining Xe atoms leave the deposit and enter the gas phase. The remaining still incorporated Xe atoms cause mild structure deformations locally, but the bulk of the MgF_2 deposit is rearranged into the rutile-type structure as if no impurities had been present. Thus, the structural features of the tempered deposit are not severely affected by the presence of such impurities (cf. Figure 3), and the remainder of the simulations described below were performed without including impurity atoms.

Deposition and Tempering on the Al_2O_3 Substrate. In this subsection, the deposition and tempering of 1:1 mixtures of MgF_2 monomers and dimers involving a total of 6681 Mg and F atoms for two different deposition rates and a number of different deposition and annealing temperatures are discussed. An overview of the different systems (i.e., a combination of the deposition rate and temperature and annealing temperature) studied is given in Table 2.

Deposition. At 1000 K, the 6681 atoms deposited on a 3600-atom α-Al_2O_3 substrate produced a film of thickness of around 75 Å, whereas for the amorphous deposit at 50 K, the thickness for the same number of atoms was 90 Å (see Figure 5). Of particular interest in the deposition and annealing process is the temperature distribution throughout the sample, in particular as a function of the height above the substrate surface.

The deposited film was analyzed using different physical quantities that include (1) the temperature gradient along the z axis, (2) coordination histograms of Mg−Mg, Mg−F, and F−F,

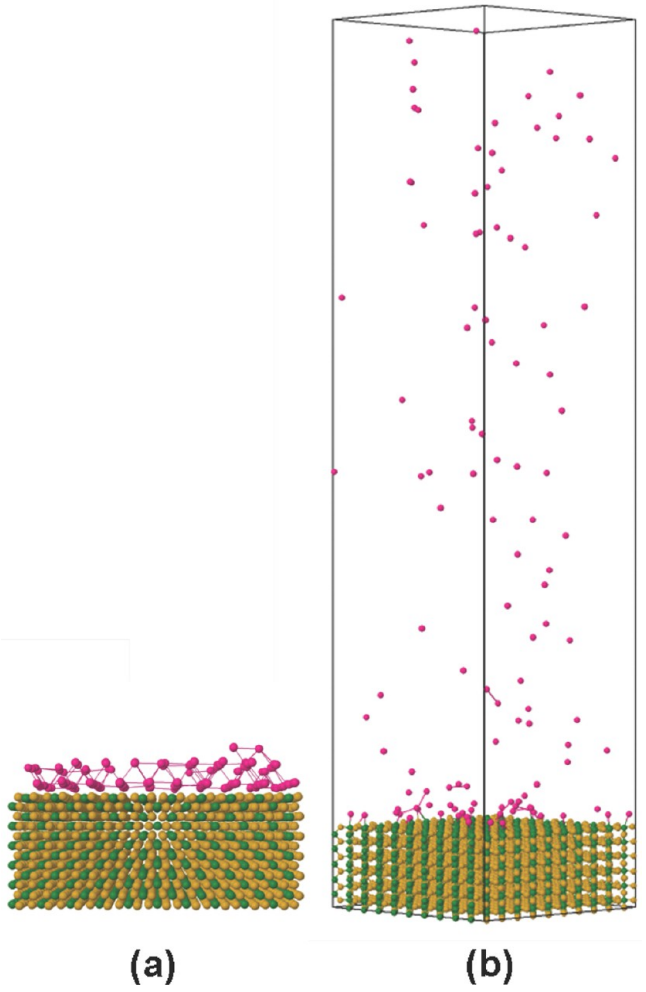

Figure 2. Deposition and annealing of inert gas atoms: (a) 119 atoms of Xe deposited at 50 K on MgF_2-rutile and then equilibrated for 30 ns; (b) after annealing the inert gas deposit for 30 ns at 1000 K. Color scheme: Mg, green; F, yellow; Xe, pink.

(3) radial distribution functions to study the long-range order, and (4) bond-distance histograms. These are shown in Figure 4. We can see that, for a deposition at 50 K, there is a positive temperature gradient across the z axis, indicating that the topmost part of the film is hotter than the substrate temperature (cf. Figure 4). This is in contrast to the previous study on Xe,[20] where the temperature was fluctuating around the average values over the deposited layers during the deposition process itself. This temperature distribution in the MgF_2 deposit is most likely the result of the fast deposition rates that had to be used in the simulation because of time considerations, together with the large amount of heat released when the atoms and molecules are adsorbed at the surface.

In all cases, we see the beginning of close-sphere packing (mostly of the hcp type) of the F atoms during the deposition itself, indicated by the peak at 12 in the F−F coordination histogram. The Mg−F bond distances are consistent with the experiment, but the spread is quite broad. Similarly, the wide range of coordination numbers seen and the lack of clear peaks in the bond angle distribution show that, during the actual deposition, no long-range order and only a limited degree of short-range order are present in the deposit, regardless of the deposition temperature or deposition rate.

dx.doi.org/10.1021/ic501499k | Inorg. Chem. 2015, 54, 782−791

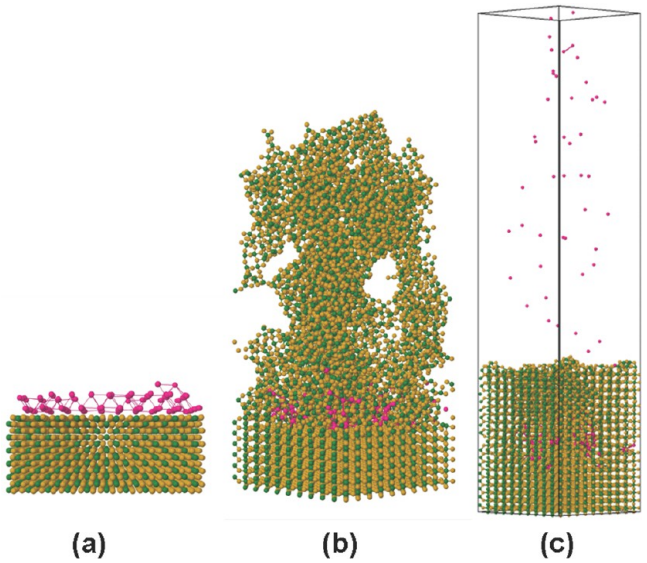

Figure 3. Deposition and annealing of MgF_2 on a Xe layer: (a) 119 atoms of Xe deposited and equilibrated on MgF_2-rutile; (b) deposition of MgF_2 monomers and dimers (6648 atoms) on the Xe layer; (c) tempering the deposit for 30 ns at 1000 K. The color scheme is like that in Figure 2.

Table 2. Summary of the Amorphous Mixtures Generated and the Gas-Phase Constituents

deposit (ratio)	temperature of substrate (K)	rate of deposition (atoms/s)	substrate
Xe	50, 300, 500, 1000	10^{11}	MgF_2-rutile
MgF_2 monomer and dimer (1:1)	50, 300, 500, 1000	10^{12}	Al_2O_3, MgF_2-rutile, MgF_2-anatase
$(MgF_2)_{10}$ and $(MgF_2)_{15}$ (1:4)	50	10^{12}	Al_2O_3
only monomer	50	10^{12}	Al_2O_3

Tempering the Deposit. After the deposition stage resulting in amorphous structures as described above for deposition at temperatures ranging from 50 to 1000 K, we tempered these deposits first at the temperatures at which these had been grown. However, even tempering at 1000 K for 18 ns did not yield an ordered deposit. Thus, in order to accelerate the rearrangement processes, we performed tempering at 1500 and 2000 K for five different amorphous structures grown at 50 K (the experimentally reported melting point of MgF_2 is 1536 K,[40] but it must be noted that most empirical potentials fitted for bulk systems do not reproduce melting points well and tend to under- or overestimate this value significantly).

For all amorphous samples studied (i.e., the ones generated using big clusters, small clusters, and various temperatures), tempering at 1500 K led to a structure exhibiting ordering within a simulation time of approximately 1 ns. By following the evolution of the system, we observe that the crucial element for the development of an ordered structure is the formation of an ordered layer at the substrate−deposit interface. As soon as this is achieved, the ordering process takes place in an approximate layer-by-layer fashion starting from the bottom of the deposit. This process can be clearly seen in the simulations at 1500 K. Figure 6 shows snapshots that clearly demonstrate this bottom-up ordering process.

The change in total energy of the system during the annealing process is depicted in Figure 7, for a typical run at 1500 K. First, the energy of the temperature deposit significantly increases during tempering as a result of an increase in the kinetic energy due to an increase in the temperature to the value at which annealing takes place. After a certain time has elapsed, the process of ordering begins and the energy reduces drastically as more and more energetically favorable bonds are formed. After about 1 ns, the system equilibrates and the bottom-up ordering process is nearly complete. We note that for runs at 2000 K crystallization does not occur because the amorphous deposit becomes liquidlike and remains in this state for the duration of the simulation.

We have seen that during deposition, for all of the choices of the deposition parameters, the temperature of the deposit increased gradually in the direction normal to the exposed plane of the substrate. During the tempering stage, however, this trend is reversed almost instantly because now the thermostat at the bottom of the substrate serves as the heat source in the system, without newly deposited clusters adding the kinetic energy at the top. The trend is illustrated in Figure 8, where we can see the change in the temperature profile as a function of the z coordinate.

Structural Features of the Annealed Deposit on α-Al_2O_3. After annealing for 1 ns at 1500 K, all structures show a predominantly hcp-like packing of F atoms, as indicated by an ABAB-type stacking of the F layers (cf. Figure 9). On the basis of the experiment, the amorphous-to-rutile phase transition has been suggested to proceed via the $CaCl_2$-type structure through an order−disorder-type phase transition. The basic idea is that there exists a random distribution of Mg atoms over the F_6 octahedral holes in the hcp packing, and this prevents, or at least slows, the $CaCl_2$-to-rutile shearing transformation. To be classified as the rutile type, the arrangement of F atoms should be that of a tetragonal close packing with an F−F coordination of 11, whereas in the $CaCl_2$-type structure, the F−F coordination should be equal to 12.

A clearer picture emerges when we analyze the ordered phases via the connectivity of the MgF_6 octahedra along the yz and xz planes, in sections of 3−4 Å thickness along the x or y directions, respectively. We see that while the ABAB-type stacking of F atoms is consistently maintained normal to the substrate throughout the whole deposit, the Mg atoms are distributed in such a way across the deposit as to enable the existence of two different locally ordered specific crystalline arrangements: MgF_2 nanocrystallites of the $CaCl_2$ type with edge- and corner-sharing MgF_6 octahedra and regions containing MgF_2 crystallites in the CdI_2-type layered arrangement of edge-connected octahedra, respectively. Both of these configurations can coexist while maintaining a common hcp arrangement of the F atoms. In fact, the CdI_2-type crystal structure had also been predicted to be a kinetically stable local minimum on the energy landscape by Wevers et al.[22,23] The polyhedral patterns are shown in Figure 10. Upon quenching of these structures using the procedure outlined in the Method section, the two distinct nuclei are clearly visible (cf. Figure 11).

As mentioned above, it has been previously argued[21] that the transition from amorphous to $CaCl_2$ to rutile is driven by the diffusion of Mg atoms within the hcp lattice of F atoms where the $CaCl_2$-type structure is stabilized by a certain amount of disorder in the occupation of the MgF_6 octahedra. This assumption was used to interpret the structural distortions in the X-ray diffraction experiments. Furthermore, transmission

dx.doi.org/10.1021/ic501499k | Inorg. Chem. 2015, 54, 782−791

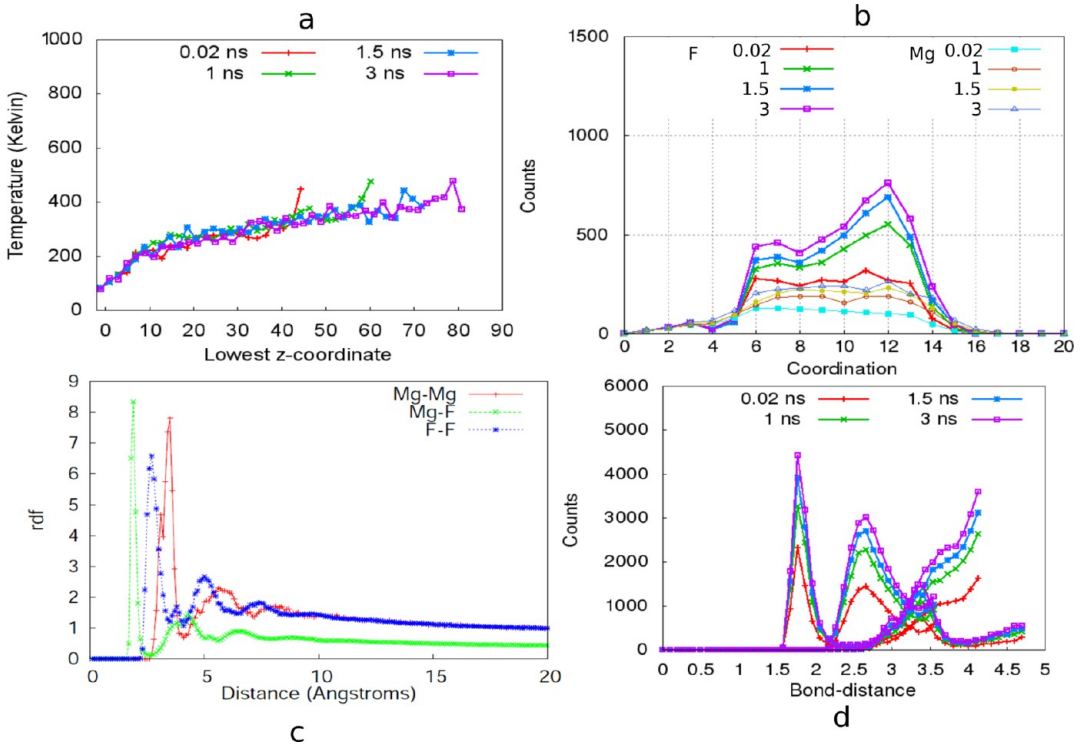

Figure 4. Analysis of the deposition at 50 K: (a) temperature in planes normal to the substrate at different time steps (0.02, 1, 1.5, and 3 ns) as a function of height z; (b) F−F and Mg−Mg coordination numbers at different time steps (0.02, 1, 1.5, and 3 ns); (c) radial distribution function for Mg−Mg, Mg−F, and F−F distances at 3 ns showing no long-range order; (d) distribution of bond distances among neighboring atoms at different time steps (0.02, 1, 1.5, and 3 ns).

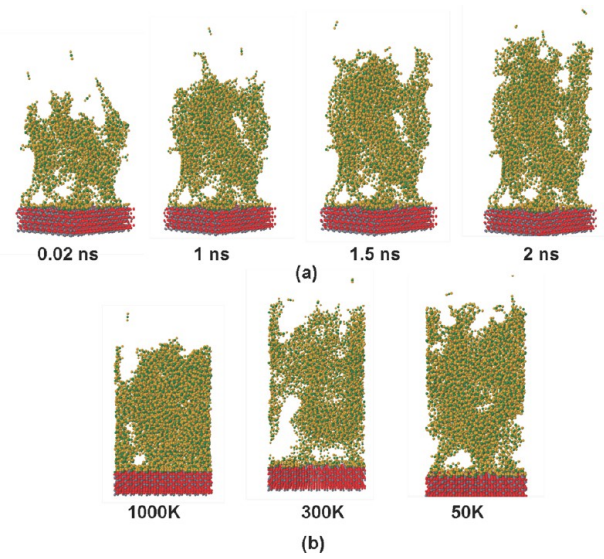

Figure 5. Deposition at different temperatures: (a) snapshots of the amorphous MgF_2 deposit at 50 K at four different times (0.02, 1, 1.5, and 2 ns); (b) final amorphous deposits at three different temperatures (1000, 300, and 50 K). The color scheme is like that in Figure 1.

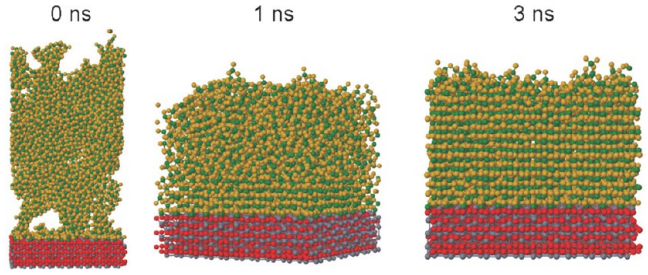

Figure 6. Snapshots of the development of the deposit during the annealing process at 1500 K at three times (0, 1, and 3 ns), starting from an amorphous deposit obtained at 50 K. The color scheme is like that in Figure 1.

electron microscopy (TEM) studies suggest that the $CaCl_2$-type nucleus is stabilized by grain boundaries,[26] but the structure of the grain boundaries has remained unclear.[26]

However, we can see from our MD simulations that there is another more appealing alternative to this mechanism. We argue that it is the presence of small regions containing the CdI_2-type nuclei that stabilizes the majority phase of $CaCl_2$ nanocrystallites. Furthermore, it would appear that the CdI_2-type layered arrangement of edge-sharing polyhedra should be a part of (or even replace) the hypothesized grain boundaries. The radial distribution functions of the model derived from experimental studies appear to match the model predicted by our MD simulations reasonably well.[26] Thus, we propose that stabilization of the $CaCl_2$-type phase occurs via intermediate nanocrystalline regions of the CdI_2 type. We note that both our simulations and the experiment show that the ABAB-type stacking of F atoms occurs first and is followed by the diffusion of Mg atoms into the octahedral holes, which, according to the simulations, results in a locally ordered deposit, exhibiting regions with $CaCl_2$- and CdI_2-type structure.

Pauling's third rule for ionic crystals[41] dictates that the $CaCl_2$-type structure should be more favorable energetically because of reduced Coulombic repulsion in edge- and vertex-sharing octahedra. Therefore, it is reasonable to expect that this crystallite would increase in size at the expense of the CdI_2-type crystallite over a long period of time. Eventually, when the

dx.doi.org/10.1021/ic501499k | Inorg. Chem. 2015, 54, 782−791

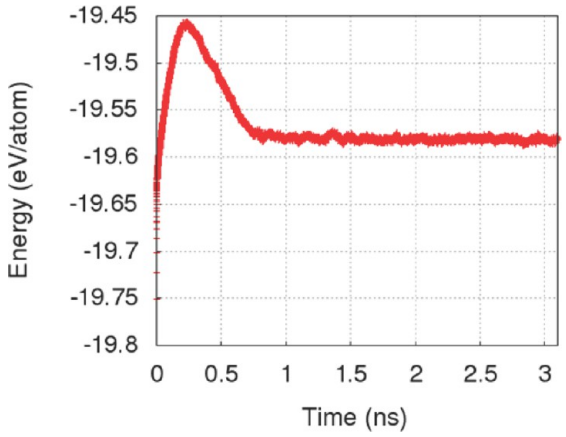

Figure 7. Typical change in the potential energy during annealing at 1500 K of an amorphous deposit constructed at 50 K. The energy increases as the substrate is heated from 50 to 1500 K. This is very quickly followed by a local ordering, resulting in ordered nanocrystallites with $CaCl_2$- and CdI_2-type nuclei, with a concomitant decrease in the potential energy.

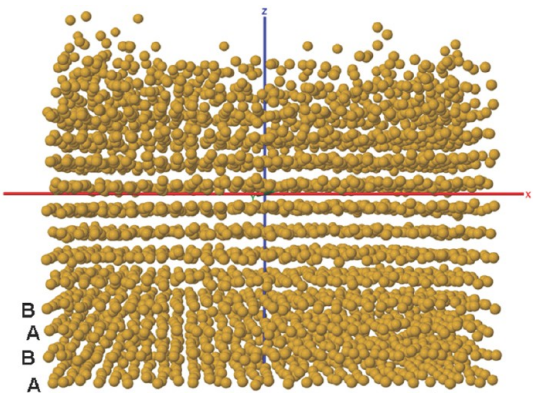

Figure 9. ABAB-type stacking of F atoms in the final annealed deposit at 1500 K after 3 ns. The Mg, Al, and O atoms are hidden from view. Both the CdI_2 and $CaCl_2$ structures are formed within this stack.

$CaCl_2$ crystal is big enough to make a C_2-axis rotation (the shearing transformation) energetically preferable in spite of the formation of (disordered) grain boundaries between the ensuing rutile crystallites, the $CaCl_2$ structure relaxes to the more stable rutile structure. This needs to be confirmed by further calculations, e.g., by performing kinetic Monte Carlo simulations on this system, in order to access the large experimental time scales that cannot be reached in the straightforward MD simulations performed in this study.

Deposition and Tempering on MgF_2 Substrates. *MgF_2-Rutile Substrate.* In order to gain additional insight into the growth of (meta)stable modifications during the LT-ABD

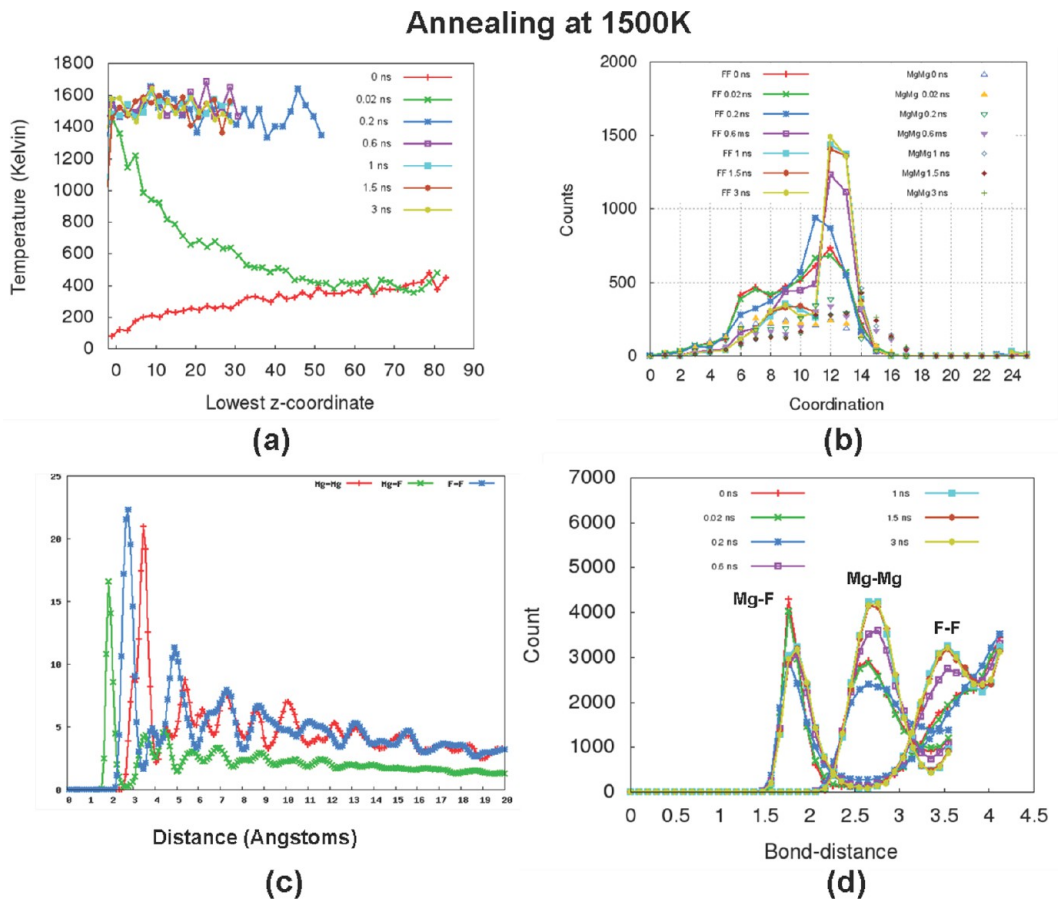

Figure 8. Analysis of annealing at 1500 K: (a) temperature in planes normal to the substrate at different time steps (0, 0.02, 0.2, 0.6, 1, 1.5, and 3 ns) as a function of the height z; (b) F−F and Mg−Mg coordination numbers at different time steps (0, 0.02, 0.2, 0.6, 1, 1.5, and 3 ns); (c) radial distribution function for Mg−Mg, Mg−F, and F−F distances at 3 ns showing long-range order; (d) distribution of bond distances among neighboring atoms at different time steps (0, 0.02, 0.2, 0.6, 1, 1.5, and 3 ns).

dx.doi.org/10.1021/ic501499k | *Inorg. Chem.* 2015, 54, 782−791

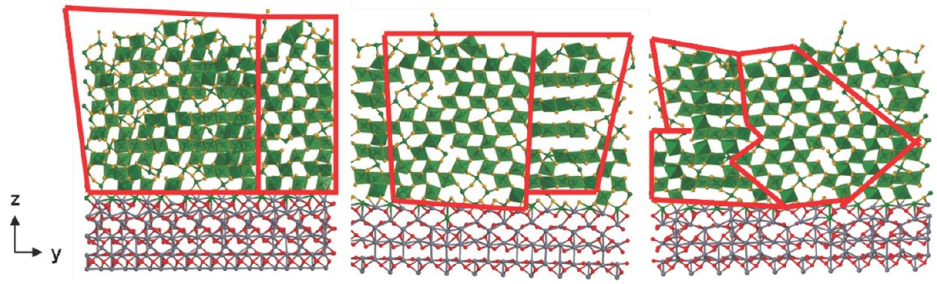

Figure 10. Emergence of two competing nuclei corresponding to the CdI_2- and $CaCl_2$-type structures in the annealed deposit at 1500 K after 3 ns. The domains are outlined in red. Sections of 3 Å width (cut across the *yz* plane) are shown. Green octahedra show six-coordinated Mg atoms with F atoms at the edges.

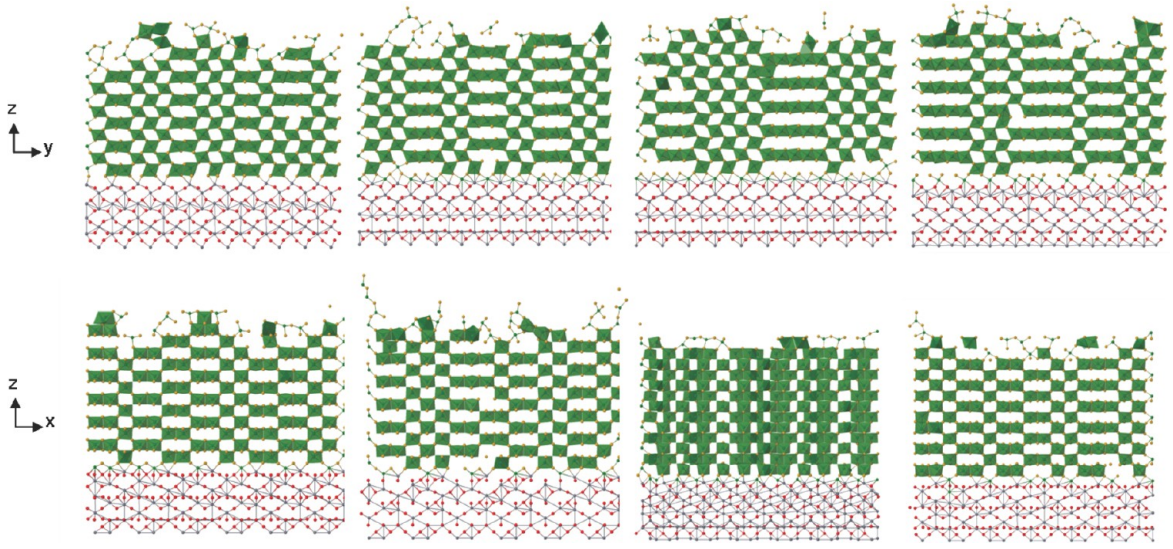

Figure 11. Clearly distinguishable nuclei of the $CaCl_2$ and CdI_2 type after quenching of the final annealed deposit from 1500 to 0.001 K. Sections of 3 Å width cut across the *yz* and *xz* planes) are shown. The color scheme is like that in Figure 10.

synthesis, we have, in addition, performed deposition and tempering studies on substrates consisting of the two modifications with the lowest energies and highest energetic barriers that had been observed on the energy landscape of MgF_2:[23] rutile and anatase. We note that, for the deposition at high temperatures, the substrate serves as a "seed crystal" of the desired modification: on the rutile substrate, the analogous process of depositing and tempering an amorphous MgF_2 phase directly results in a rutile crystal. In particular, we see no formation of a $CaCl_2$-type phase or stacking faults that lead to the CdI_2-type nanosized structures on the Al_2O_3 substrate. As expected from reasoning by analogy to MBE studies, we observe epitaxial growth of the rutile phase at temperatures of 1000 K and the generation of (partly) amorphous deposits at temperatures below 500 K. These simulated structures obtained on the rutile-type substrate were systematically matched with pair distribution functions obtained from TEM studies. Further details of this comparison can be found in ref 26.

MgF_2-Anatase Substrate. The yet-unknown anatase-type polymorph of MgF_2 is predicted to be the second most energetically favorable structure for MgF_2 at standard conditions.[23,24] In this earlier work, using a combination of Monte Carlo simulated annealing and threshold runs, it had been found that this particular polymorph of MgF_2 corresponds to an isolated basin on the energy landscape separated by a high energetic and entropic barrier from other polymorphs. In order to estimate the stability of this modification and to explore the likelihood that an anatase polymorph of MgF_2 might be accessible via the LT-ABD method, we have studied the deposition and growth of MgF_2 on a substrate exhibiting the hypothetical anatase structure. From the energy-landscape exploration on bulk MgF_2, ab initio local optimizations and the vibrational spectra of MgF_2-anatase, we can state with confidence that the anatase structure should be kinetically stable, at least at very low temperatures. However, the degree of kinetic stability of this structure at high temperatures still needs to be established. We note that we did not come across this structure during the amorphous-to-crystalline phase transition on Al_2O_3 discussed above.

We chose to expose the (011) and (100) faces based on studies in the literature[42,43] on the stability of the TiO_2-anatase structure and electronic structure calculations of surface energies using the *CRYSTAL'09* suite. For the purpose of studying epitaxial growth, we feel it would be sufficient to explore low-index surfaces only.

Using a combination of Monte Carlo simulated annealing and threshold runs, it had been found that this particular polymorph of MgF_2 corresponds to an isolated basin on the energy landscape separated by a high energetic and entropic barrier from other polymorphs. In order to estimate the stability of this modification and to explore the likelihood that an anatase polymorph of MgF_2 might be accessible via the LT-

dx.doi.org/10.1021/ic501499k | *Inorg. Chem.* 2015, 54, 782−791

ABD method, we have studied the deposition and growth of MgF_2 on a substrate exhibiting the hypothetical anatase structure. From the energy-landscape exploration on bulk MgF_2, ab initio local optimizations, and the vibrational spectra of MgF_2-anatase, we can state with confidence that the anatase structure should be kinetically stable, at least at very low temperatures. However, the degree of kinetic stability of this structure at high temperatures still needs to be established. We note that we did not come across this structure during the amorphous-to-crystalline phase transition on Al_2O_3 discussed above (Figure 12).

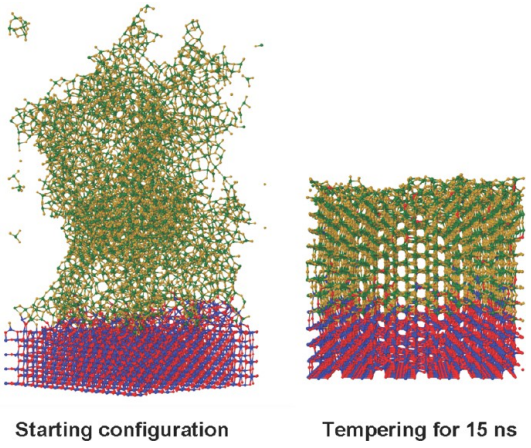

Figure 12. Annealing on MgF_2-anatase: Tempering the amorphous deposit for 15 ns at 1500 K on the anatase-110 substrate resulting in the formation of the anatase-type structure. The color scheme is like that in Figure 1.

For the (011) slab, the starting structure was terminated by F atoms and comprised 3360 atoms. The simulation cell dimensions were 53.50 Å × 52.22 Å in the x and y directions, respectively. The MgF_2-anatase unit cell used to produce this slab had dimensions of a = 3.822 Å, b = 3.822 Å, and c = 9.719 Å. After tempering the slab for 2 ns at 1000 K, we saw a significant relaxation of the topmost layer of F atoms, quite similar to the case of Al_2O_3 described above. The starting and final structures at 1000 K are shown in Figure 1. This is the highest temperature at which these slabs were equilibrated.

The (100) slab comprised 3120 atoms and the topmost layer consisted of both Mg and F atoms. The simulation cell dimensions were 48.59 Å × 49.69 Å in the x and y directions, respectively. Here, also, we see a significant relaxation of the topmost layer of the substrate, which is most pronounced at 1000 K, as can be seen from Figure 1. Thus, assuming that we are able to stabilize a big enough nucleus experimentally, our MD simulations of the substrate slab show that the anatase modification of the MgF_2 structure should survive long enough as a metastable phase for experimental observation.

The second step of this investigation consisted of the deposition of 6000 atoms on the substrate at various temperatures. During deposition on anatase [(110) and (100)] substrates at 1000 K, we find epitaxial growth of the anatase structure. At 500 K, the growth is still toward an overall anatase structure but with a certain amount of disorder. At low temperatures of 10 and 50 K, there is practically no diffusion during the deposition and thus we get amorphous deposits on all surfaces studied. This suggests that depositing at high temperatures on an anatase-compatible substrate might increase the likelihood of obtaining the anatase form. Furthermore, the fact that the deposition process at 1000 K does not lead to the formation of, e.g., rutile-like regions also underlines the kinetic stability of this anatase structure. To test this proposition further, we annealed the amorphous structures obtained after deposition at low temperatures at a high temperature of 1500 K for 18 ns. On both anatase surfaces studied [(100) and (011)], the amorphous structure transforms to the anatase-type structure of the substrate within 2.1 ns. We can thus conclude that if a big enough seed of the anatase type is formed, this structure can be stabilized for the MgF_2 system.

In this context, we recall that, with the exception of the two bottom-most layers, the substrate atoms are free to move as well. As a consequence, some of the substrate atoms may diffuse into and are incorporated in the (nanocrystalline) deposit, and, of course, the converse process may happen also. Comparing the two MgF_2 substrates, we note that this effect is much more noticeable for anatase than for rutile, which is a reflection of the higher overall thermodynamical stability of the rutile modification.[42] Nevertheless, even though the anatase system was exposed to temperatures high enough to induce widespread interdiffusion and atom exchange, it remained in the anatase phase, and there was no indication of an impending transformation to an alternative modification. In contrast to the two MgF_2 substrates, no interdiffusion took place in any of the simulations where MgF_2 was deposited on the sapphire substrate. This is not unexpected because neither are the applied temperatures high enough to induce noticeable movement of the substrate atoms as such nor are the two chemical systems similar enough to favor such atom-exchange processes on the time scale of our simulations.

CONCLUSION

In this study, we have strived to thoroughly model the LT-ABD synthesis of MgF_2. Investigating the effect of neutral surface impurity molecules and atoms at the example of Xe atoms, we find that their presence does not have a significant impact on the amorphous-to-crystalline transition in MgF_2. We have generated amorphous deposits of MgF_2 via the deposition of various $(MgF_2)_n$ clusters on a sapphire α-Al_2O_3 substrate with the 0001 surface exposed that were subsequently annealed at elevated temperatures. Upon annealing, the amorphous deposits order in a bottom-up manner, leading to the emergence of two competing nanocrystalline modifications, exhibiting CdI_2- and $CaCl_2$-type structures that are not kinetically stable on the macroscopic level. While the former modification had been observed recently as a metastable transitory phase during LT-ABD experiments, the CdI_2-type structure has not yet been observed experimentally for the MgF_2 system but had been predicted to exist in earlier work. We show that the joint growth of CdI_2- and $CaCl_2$-type nanocrystalline phases explains stabilization of the $CaCl_2$-type modification as a metastable phase in the LT-ABD experiment. Finally, the in-principle feasibility of the synthesis of the predicted but yet unknown anatase-type polymorph of MgF_2 and its kinetic stability was demonstrated by depositing MgF_2 clusters on a hypothetical MgF_2-anatase substrate and annealing the resulting amorphous deposit.

AUTHOR INFORMATION

Corresponding Author

*E-mail: s.neelamraju@bham.ac.uk.

Present Address

‡S.N.: School of Chemistry, University of Birmingham, Edgbaston B15 2TT, U.K.

Notes

The authors declare no competing financial interest.

■ ACKNOWLEDGMENTS

S.N. is thankful for DFG Project 1415 (Crystalline Non-equilibrium Phases: Theory and Experiment) for financial support.

■ REFERENCES

(1) Schön, J. C.; Jansen, M. *Angew. Chem., Int. Ed. Engl.* **1996**, *35*, 1286−1304.
(2) Woodley, S. M.; Battle, P. D.; Gale, J. D.; Catlow, C. R. A. *Phys. Chem. Chem. Phys.* **1999**, *1*, 2535−2542.
(3) Schön, J. C.; Jansen, M. *Z. Kristallogr.* **2001**, *216*, 307−325, 361−383.
(4) Oganov, A. R.; Glass, C. W. *J. Chem. Phys.* **2006**, *124*, 244704.
(5) Pickard, C. J.; Needs, R. J. *Phys. Rev. Lett.* **2006**, *97*, 045504.
(6) Doll, K.; Schön, J. C.; Jansen, M. *Phys. Chem. Chem. Phys.* **2007**, *9*, 6128.
(7) Woodley, S. M.; Catlow, C. R. A. *Nat. Mater.* **2008**, *7*, 937.
(8) Ozolins, V.; Majzoub, E. H.; Wolverton, C. *Phys. Rev. Lett.* **2008**, *100*, 135501.
(9) Schön, J. C.; Jansen, M. *Int. J. Mater. Res.* **2009**, *100*, 135−152.
(10) Jansen, M. *Angew. Chem., Int. Ed.* **2002**, *41*, 3747−3766.
(11) Fischer, D.; Jansen, M. *Angew. Chem., Int. Ed.* **2002**, *41*, 1755−1756.
(12) Harris, F. R.; Standridge, S.; Feik, C.; Johnson, D. C. *Angew. Chem., Int. Ed.* **2003**, *42*, 5296−5299.
(13) Fischer, D.; Čančarevič, Ž.; Schön, J. C.; Jansen, M. *Z. Anorg. Allg. Chem.* **2004**, *630*, 156−160.
(14) Santamaria-Perez, D.; Haines, J.; Amador, U.; Moran, E.; Vegas, A. *Acta Crystallogr., Sect. B* **2006**, *62*, 1019−1024.
(15) Catlow, C. R. A., DeLeeuw, N. H., Anwar, J., Davey, R. J., Roberts, K. J., Unwin, P. R., Eds. *Faraday Discuss. 136: Crystal Growth and Nucleation*; Royal Society of Chemistry: London, 2007.
(16) Fischer, D.; Jansen, M. *J. Am. Chem. Soc.* **2002**, *124*, 3488.
(17) Fischer, D.; Jansen, M. *Z. Anorg. Allg. Chem.* **2003**, *629*, 1934.
(18) Liebold-Ribeiro, Y.; Fischer, D.; Jansen, M. *Angew. Chem., Int. Ed.* **2008**, *47*, 4428−4431.
(19) Bach, A.; Fischer, D.; Jansen, M. *Z. Anorg. Allg. Chem.* **2009**, *635*, 2406−2409.
(20) Toto, N.; Schön, J. C.; Jansen, M. *Phys. Rev. B* **2010**, *82*, 115401.
(21) Bach, A.; Fischer, D.; Mu, X.; Sigle, W.; van Aken, P. A.; Jansen, M. *Inorg. Chem.* **2011**, *50*, 1563−1569.
(22) Wevers, M. A. C.; Schön, J. C.; Jansen, M. *J. Solid State Chem.* **1998**, *136*, 223−246.
(23) Wevers, M. A. C.; Schön, J. C.; Jansen, M. *J. Phys.: Condens. Matter* **1999**, *11*, 6487−6499.
(24) Schön, J. C.; Wevers, M.; Jansen, M. *J. Phys. A: Math. Gen.* **2001**, *34*, 4041−4052.
(25) Neelamraju, S.; Bach, A.; Schön, J. C.; Fischer, D.; Jansen, M. *J. Chem. Phys.* **2012**, *137*, 194319.
(26) Mu, X.; Neelamraju, S.; Sigle, W.; Koch, C. T.; Totò, N.; Schön, J. C.; Bach, A.; Fischer, D.; Jansen, M.; van Aken, P. A. *J. Appl. Crystallogr.* **2013**, *46*, 1105−1116.
(27) Neelamraju, S.; Schön, J. C.; Doll, K.; Jansen, M. *Phys. Chem. Chem. Phys.* **2012**, *14*, 1223−1234.
(28) Bacorisen, D.; Smith, R.; Ball, J.; Grimes, R.; Uberuaga, B.; Sickafus, K.; Rankin, W. *Nucl. Instrum. Methods Phys. Res., Sect. B* **2006**, *250*, 36−45.
(29) Catti, M.; Pavese, A.; Dovesi, R.; Roetti, C.; Causa, M. *Phys. Rev. B* **1991**, *44*, 3509−3517.
(30) Wolf, D.; Keblinski, P.; Phillpot, S. R.; Eggebrecht, J. *J. Chem. Phys.* **1999**, *110*, 8254−8282.
(31) Heinz, T. N.; Hünenberger, P. H. *J. Comput. Chem.* **2004**, *25*, 1474−1486.
(32) Schön, J. C.; Jansen, M. *Comput. Mater. Sci.* **1995**, *4*, 43−58.
(33) Harrison, W. A. *Solid State Theory*; W. H. Freeman and Co.: San Francisco, 1980.
(34) Verdozzi, C.; Jennison, D. R.; Schultz, P. A.; Sears, M. P. *Phys. Rev. Lett.* **1999**, *82*, 799−802.
(35) Kelber, J.; Niu, C.; Shepherd, K.; Jennison, D.; Bogicevic, A. *Surf. Sci.* **2000**, *446*, 76−88.
(36) Vassilyeva, A.; Eglitis, R.; Kotomin, E.; Dauletbekova, A. *Cent. Eur. J. Phys.* **2011**, *9*, 515−518.
(37) Kirkpatrick, S.; Gelatt, C. D., Jr.; Vecchi, M. P. *Science* **1983**, *220*, 671−680.
(38) Schön, J. C. *Ber. Bunsenges.* **1996**, *100*, 1388−1391.
(39) An exception would be H_2O, of course, which would result in the formation of hydroxyl groups at the surface of Al_2O_3.
(40) Lide, D. P., Ed. *CRC Handbook of Chemistry and Physics*, 81st ed.; CRC Press: Boca Raton, FL, 2000.
(41) Müller, U. *Inorganic Structural Chemistry; Inorganic Chemistry*; John Wiley & Sons: New York, 1993.
(42) Beltran, A.; Sambrano, J.; Calatayud, M.; Sensato, F.; Andres, J. *Surf. Sci.* **2001**, *490*, 116−124.
(43) Lazzeri, M.; Vittadini, A.; Selloni, A. *Phys. Rev. B* **2001**, *63*, 155409.
(44) A second reason might be that the anatase surface is more irregular than the rutile surface, leading to a lower stability of the surface layer and thus to an effectively lower kinetic stability of anatase at elevated temperatures.